PROCEEDINGS OF ECOS 2023 - THE 36TH INTERNATIONAL CONFERENCE ON
EFFICIENCY, COST, OPTIMIZATION, SIMULATION AND ENVIRONMENTAL IMPACT OF ENERGY SYSTEMS
25-30 JUNE, 2023, LAS PALMAS DE GRAN CANARIA, SPAIN

Modelling and performance analysis of a Low Temperature A-CAES system coupled with renewable energy power plants

Francesca Carolina Marcello[a], Davide Micheletto[b], Daniele Cocco[b] and Vittorio Tola[b]

[a] Dept. of Mechanical, Chemical and Materials Engineering, University of Cagliari, Cagliari, Italy, francescac.marcello@unica.it
[b] Dept. of Mechanical, Chemical and Materials Engineering, University of Cagliari, Cagliari, Italy

Abstract:
The ever-increasing electricity production from non-programmable Renewable Energy Sources (RES) requires flexible and sustainable solutions for energy storage. In this paper, the design, and the performance of a Low Temperature Adiabatic Compressed Air Energy Storage (LTA-CAES) system are presented. The design of this system is optimised to better utilise the energy produced by either a photovoltaic (PV) power plant and an onshore wind farm in order to meet the energy demand of a small town of about 10,000 inhabitants, considered as the case study. To ensure efficient operation of the turbomachines, the mass flow rate during both the charge and discharge phases was fixed, allowing most of the compressors and turbines to operate at design conditions. Two packed-bed Thermal Energy Storage (TES) systems are used to store the thermal energy produced during the compression phase: the first exchanges heat directly with the compressed air, while the second uses Therminol-66 as a heat transfer fluid. A mathematical model of the LTA-CAES system was developed using MATLAB/Simulink to simulate its performance, considering the off-design behaviour of the turbomachines and the TES systems over a year. The results demonstrate that the LTA-CAES system increases the share of the yearly energy demand covered by renewable energy, from 41.8% to 60.7% when coupled with the PV plant, and from 48.0% to 56.5% when coupled with the wind farm.
Keywords:
Adiabatic Compressed Air Energy Storage (A-CAES); LTA-CAES; Energy Storage; Renewable Energy Sources; Thermal Energy Storage.

1. Introduction

The intermittent nature of Renewable Energy Sources (RES) results in significant fluctuations in energy production, often not aligned with the power demand of the end-users. Balancing the production and consumption of electrical energy is a highly debated issue, especially as RES penetration in the grid increases. To address this issue, various energy storage systems were developed, including chemical, electrochemical, mechanical, electrical and thermal storage systems [1]. Among the energy storage technologies characterised by medium-high storage capacities, Compressed Air Energy Storage (CAES) systems are one of the most promising options, with a lower cost per kWh than batteries [2], and comparable to pumping hydro systems. The system works by using a compressor to convert electrical energy into compressed air, which is stored in a reservoir. Later on, the process can be reversed by expanding the high pressure air through a turbine, generating electricity. However, one of the biggest challenges in the widespread adoption of CAES technology is the need for suitable reservoirs to store high-pressure air. For this reason, CAES plants are a promising option in regions with geological formations or disused mines. In particular, the island of Sardinia presents an ample availability of primary energy sources like solar and wind and numerous disused mines, potentially suitable for the storage of compressed air. Therefore, CAES plants are a very interesting option to repurpose a disused mine by storing the surplus energy generated by an RES plant and enhance the energy self-consumption of an end-user, such as small communities in the same area.

CAES configurations can be classified as Diabatic CAES (D-CAES), which is the first to be developed, Adiabatic CAES (A-CAES), and Isothermal CAES (I-CAES) [3]. In D-CAES systems, electrical energy is utilised by the compression train to compress the air, which is stored in a suitable reservoir. The compressed air is subsequently heated by using fossil fuels in a combustion chamber and expanded in the turbine train, generating electricity. In the I-CAES configuration, both the compression and expansion processes occur at approximately constant temperature, allowing an increase in the efficiency of the cycle. In the A-CAES configuration, a Thermal Energy Storage (TES) unit is utilised to store the thermal energy recovered by cooling the compressed air; the stored thermal energy is subsequently used to heat the air before expansion, thus

https://doi.org/10.52202/069564-0187

eliminating the need for the combustion section. As a result, an A-CAES plant is characterised by very low emissions, and it is well suited to be coupled with an RES power plant. Adiabatic CAES plants can operate at different TES temperatures and, in general, they can be divided into high-temperature (HTA-CAES) and low-temperature (LTA-CAES) systems. As described by Wolf and Budt [4], the round-trip efficiency tends to increase with the maximum temperature, but high-temperature systems are limited by the availability of suitable components. In fact, HTA-CAES systems operate at high temperature (around 600 °C) and high pressure (around 70 bar), leading to significant thermal and mechanical stress on the TES equipment, while LTA-CAES systems operate at lower temperatures (100 – 200 °C) and at atmospheric pressure. Due to limitations of the current centrifugal compressor technology, temperatures in the order of 600 °C cannot be achieved. As a result, the use of heat exchangers is necessary to maintain lower temperatures.

In the field of A-CAES systems, Grazzini and Milazzo [5] proposed one of the first models, characterised by a variable configuration system allowing for compressors and turbines to be arranged in different series and parallel configurations, to achieve the desired air pressure and charge time. A significant benefit of the system was the ability to use commercially available components. Hartmann et al. [6] investigated various configurations for A-CAES plants and concluded that the highest round-trip efficiencies are achieved with a two-stage compressor train and by reaching high temperatures in the thermal energy storage system, upwards of 600 °C. Wolf and Budt [4] designed an LTA-CAES system utilising multistage radial compressors and expanders with intermediate cooling, and storage temperatures ranging from 95 °C to 200 °C with a non-thermocline two-tank system. The system was estimated to reach a round-trip efficiency of 52 – 60%, with a start-up time of less than 5 minutes. Wang et al. [7] presented the results of the first experimental setup for an LTA-CAES, featuring a 5-stage compressor train and a 3-stage expansion train. Heat exchangers were utilised to transfer heat between air and water. The thermal energy generated during the charge phase was stored in two water tanks, while the air compressed at 9.34 MPa was stored in two steel tanks. The round-trip efficiency of the system was reported to be 22.6%. Budt et al. [3] devised a techno-economical model that utilises reversible turbo and piston machinery to reduce the capital cost of the LTA-CAES plant, resulting in enhanced competitiveness. They proposed a modular design, with a 2 MW_{el} compressor power input for each module. These modules can be coupled with any compressed air storage volume, whether natural (such as a cave) or artificial (such as tanks or pipes). In their study, Zhang et al. [8] examined an A-CAES system that employs a variable configuration in order to accommodate fluctuations in the production profile of a wind farm in China. The system consists of a 4-stage centrifugal compressor, a 4-stage radial expander and two pressure reservoirs (a low-pressure and a high-pressure one). The variable configuration enables the compressors and the expanders to operate under various modes, thus extending the operational range of the A-CAES. The authors reported that this system increases the wind power capacity factor from 26.29% to 71.02%. Arabkoohsar et al. [9] investigated the impact of part-load operation on the overall performance of an LTA-CAES, utilising real performance maps of all system components. For optimal efficiency, the energy storage system must operate close to design conditions. At nominal conditions, the round-trip efficiency can reach up to 68% at full load, while at 50% and 10% loads, the efficiency decreases to 52% and 28%, respectively.

The LTA-CAES configuration proposed in this work was developed with the aim of maximising the electrical energy utilisation between an RES power plant and a small town located in the south-west of Sardinia, a region with many decommissioned mining tunnels. The LTA-CAES was developed with the aim of utilising components already available on the market. To maximise the round-trip efficiency, the plant operation was studied by operating the turbomachines at mostly constant design conditions during both the charging and discharge phases. Moreover, differently from most LTA-CAES configurations, that typically incorporate a heat exchanger after each compressor to recover the thermal energy from the compressed air using a heat transfer fluid [10], this study proposes the use of two different TES units. In the first TES, the air stream directly exchanges heat with the storage material, thus eliminating the need for two heat exchangers, resulting in a more efficient heat transfer process. The second TES uses a thermal oil as a heat transfer fluid and therefore operates at low pressure. To study the operation of the LTA-CAES system integrated with RES power generation plants, a mathematical model was developed to simulate the performance of the system over an entire year. The model takes into account the off-design performance of the turbomachines, the TES units, and the heat exchangers. In this paper, the plant configuration, the mathematical models, the energy management strategy and the optimization method are described in detail. Moreover, the performance of the of the plant is then presented and discussed with reference to a case study.

2. Materials and methods

In this chapter, the configuration of the plant and the mathematical modelling of its components are presented. Moreover, the power demand and production profiles for the end-user and the RES power plants are discussed, with a description of the energy management strategy and of the optimization problem.

2.1. System description

The configuration of the LTA-CAES plant is presented in Fig 1. The power required by the end-user can be supplied either by the RES power plant, by the grid, or by the LTA-CAES plant itself. The plant operates in a

cyclical manner, with the excess energy produced by the RES plant used to compress the air, which is later used by the turbine when the end-user demand exceeds the RES production. When the LTA-CAES output power is higher than the end-user demand, part of the electrical energy is sent to the grid. The plant includes three main sections: the compression section, the expansion section, and the energy storage section. In the compression section, the air is compressed using four centrifugal compressors. The multistage low-pressure compressor (LPC) and the two multistage medium-pressure compressors (MPC1 and MPC2) are driven by the motor M1, while the single-stage centrifugal high-pressure compressor (HPC) is driven by the motor M2. Two intercoolers, IC1 and IC2, are located at the outlet side of MPC1 and MPC2 respectively, to cool the air by using thermal oil (Therminol-66) [13]. The energy storage section includes the TES system and the underground Compressed Air Storage (CAS) cavern. The TES system is based on two different thermocline packed-bed units, which are utilised to store the thermal energy recovered by cooling the compressed air. The TES1 unit exchanges heat directly with the air stream while the TES2 utilises the thermal oil as heat-transfer fluid (HTF). The heat transfer oil is stored at low temperature (25 °C) in a dedicated tank, and operates in a closed loop system, flowing through the heat exchangers on the compression and expansion sides during the charge and discharge phases, respectively. Both TES units are filled with gravel, selected for its low cost and widespread availability. At the outlet of the compression train, the high-pressure air is stored in an underground cavern obtained from a decommissioned coal mining tunnel. The expansion section of the plant includes three turbines. The high-pressure turbine (HPT), the medium-pressure turbine (MPT), and the low-pressure turbine (LPT) are connected to the generator G1. To maintain a constant mass flow rate during the discharge phase, the turbine inlet pressure is regulated using three valves, V1, V2, and V3. Two heat exchangers, HX1 and HX2, are utilised to heat the air before expansion. The aftercoolers AC1, AC2, AC3, AC4, and AC5 are used to regulate the temperature in some key sections of the plant and to ensure proper operation of the downstream components.

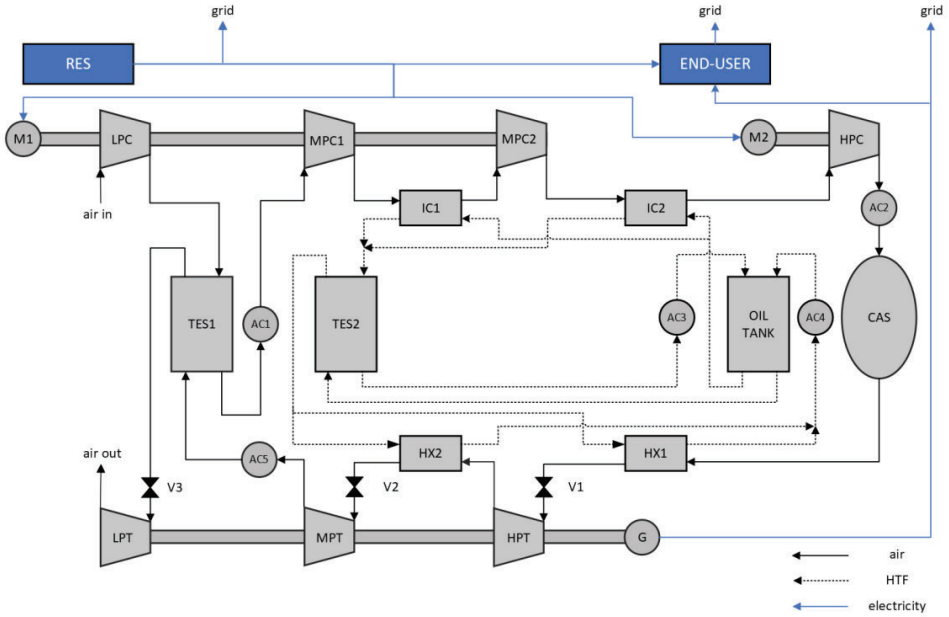

Figure. 1. Functional scheme of the LTA-CAES plant.

During the charge phase, the pressure inside the storage cavern increases, with a corresponding increase of the pressure ratio of the compression train, leading to off-design operating conditions. To mitigate this effect, the plant was designed to keep the air mass flow rate constant during the charge phase. Moreover, the LPC, MPC1, and MPC2 operate with a constant pressure ratio while the HPC regulates the pressure in the cavern by varying its rotational speed. For this reason, LPC, MPC1, and MPC2 are driven by the fixed-speed motor M1, while the HPC is driven by the motor M2 which can vary its rotational speed. The maximum pressure in the cavern is set to 100 bar, while the minimum pressure, which is strictly related to the minimum pressure ratio of the HPC, is set to 70 bar. During the discharge phase, the pressure at the inlet side of each turbine is regulated by a throttling valve.

2.2. Mathematical model

In the present section, the mathematical model used to simulate the LTA-CAES plant is presented. The mathematical models were developed on Matlab/SIMULINK by solving the mass and energy balances of all plant components and of the overall system for each time step (15 minutes, in this case) of the year.

https://doi.org/10.52202/069564-0187

2.2.1. Compressor model

The Casey and Robinson method [11] was utilised to estimate the design and off-design performance of the compressors. For each compressor, the number of stages is determined by equally dividing the enthalpy difference between the stages. With the Casey and Robinson method, the pressure ratio, the tip Mach number, the polytropic efficiency, and the non-dimensional factors were calculated for each stage of the compressor. The power required by each compressor, is calculated as:

$$P_c = \dot{m}_{air,ch} \frac{\gamma}{\gamma - 1} R_{air} T_{c,in} \left(\beta_c^{\frac{\gamma-1}{\gamma \eta_c}} - 1 \right) \quad (1)$$

Where $\dot{m}_{air,ch}$ is the mass flow rate of the compressor during the charge phase, γ is the specific heat ratio, R_{air} is the gas coefficient of air, $T_{c,in}$ is the temperature at the inlet side of the compressor, β_c is the pressure ratio of the compressor, and η_c is the polytropic efficiency of the compressor.

All compressors were designed imposing a maximum outlet temperature of 200 °C. The main performance parameters of the compressors are listed in Table 1.

Table 1. Main performance parameters of the compressors.

	LPC	MPC1	MPC2	HPC (design)
Pressure ratio	4.38	3.55	3.43	1.72
Number of stages	3	3	3	1
Inlet pressure [bar]	1.00	4.38	35.00	53.33
Outlet pressure [bar]	4.38	35.00	53.33	91.73
Inlet temperature [°C]	15	35	35	35
Outlet temperature [°C]	199.64	199.23	199.78	110.26
Polytropic efficiency	0.85	0.86	0.86	0.81

For the LPC, the inlet temperature is equal to the atmospheric temperature, set to 15 °C. For the other compressors, the two intercoolers are utilised to reduce the compressor inlet temperature to 35 °C. The HPC maps are shown in Fig 2, in terms of pressure ratio (a) and polytropic efficiency (b) as a function of the mass flow rate and the rotational speed. The blue circle indicates the design point, while the operational range of the compressor is highlighted by the double headed arrow. During the charge phase, the pressure ratio is controlled by varying the rotational speed. As shown by Fig 2, for a fixed mass flow rate, the compressor work point moves by changing the rotational speed between 70% and 110% of the design speed. The maps are generalized with the reference values, i.e., the design values. In Fig 2(b), can be observed that, at very low rotational speeds, the efficiency decreases rapidly. As a low-pressure ratio drastically reduces the efficiency, the minimum storage pressure was set to 70 bar.

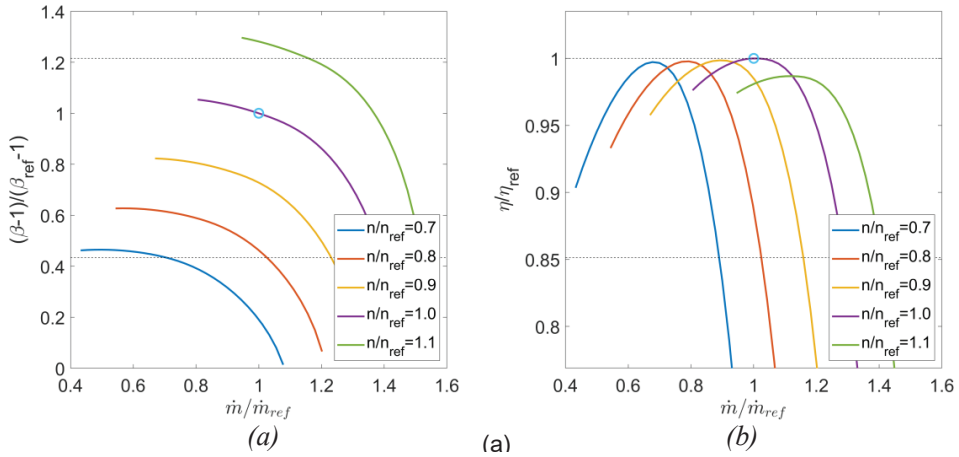

Figure. 2. High pressure compressor maps, with (a) generalised pressure ratio and (b) generalised efficiency as a function of the generalised mass flow rate for different rotational speeds.

2.2.2. Turbine model

The power produced by each turbine is calculated as:

$$P_t = \dot{m}_{air,dis} \frac{\gamma}{\gamma - 1} R_{air} T_{t,in} \left(1 - \beta_t^{\frac{\gamma-1}{\gamma} \eta_t} \right) \quad (2)$$

Where $\dot{m}_{air,dis}$ is the mass flow rate of the turbines, $T_{t,in}$ is the temperature at the inlet of the turbine, β_t is the turbine expansion ratio, and η_t is the polytropic efficiency of the turbine.

The design of the three turbines was based on [12], assuming a polytropic efficiency of 0.86 for each turbine. Throughout the discharge phase, as the pressure in the cavern decreases, a throttling valve located at the inlet side of each turbine regulates the pressure in order to maintain constancy in the mass flow rate and the reduced mass flow rate. The valves also account for the temperature variation caused by the thermocline profile of the TES units. Hence, the turbines operate in a choked flow condition throughout the entire discharge phase, achieving maximum efficiency.

The throttling valve model is based on the calculation of the reduced mass flow rate $\dot{m}_{rid}$, expressed as:

$$\dot{m}_{rid} = \dot{m}_{air,ch} \frac{\sqrt{T_{in}}}{p_{in}} \quad (3)$$

Where T_{in} and p_{in} are the inlet temperature and pressure.

2.2.3. Heat exchanger model

The following equations allow to calculate the thermal power and the heat transfer area of the heat exchangers:

$$\dot{Q} = \dot{m}_{air} c_{p,air} (T_{air,out} - T_{air,in}) \quad (4)$$

$$A = \frac{\dot{Q}}{U \, \Delta T_{ML}} \quad (5)$$

Where $\dot{Q}$ is the exchanged thermal power, $\dot{m}_{air}$ the mass flow rate of air, $T_{air,out}$ and $T_{air,in}$ are the outlet and inlet air temperature, respectively, A is the heat exchange area, U is the heat transfer coefficient, and ΔT_{ML} is the logarithmic temperature difference.

Two intercoolers recover the heat from the MPC1 and MPC2 allowing to store the produced thermal energy inside the TES2. Therminol-66 was selected as the heat transfer fluid because of its maximum temperature of 345 °C [13]. The intercoolers were designed to keep an outlet temperature of the hot fluid (air) at 35 °C assuring a steady inlet temperature for the compressors. Moreover, the approach temperature and the heat transfer coefficient were set to 10 °C, and $0.2 \, \frac{kW}{m^3 K}$, respectively [14].

The heat exchangers on the expansion side were designed to account for fluctuations in inlet pressure and temperature of the air during the discharge phase. This was achieved by using the same equations and parameters applied to the intercoolers and considering the lowest exchangeable thermal power $\dot{Q}$.

2.2.4. Thermal Energy Storage model

The volume of the TES tank is then calculated as:

$$V_{TES} = \frac{m_s}{\rho_b (1 - \epsilon)} \quad (6)$$

Where ρ_b is the density of the filler material, ϵ is the void fraction and m_s is the mass of the filler material, calculated based on the energy balance of the TES between the charge and discharge phases. A system of two equations, derived from the model developed in [15], is used to describe the operation of the two thermal energy storage (TES) units. The temperature of solid bed (T_b) and the heat transfer fluid (T_f), calculated in the direction of the air flow, are determined with the following equations (7) and (8):

$$\frac{\partial T_f}{\partial t} + \frac{G\gamma}{\rho_f \epsilon} \frac{\partial T_f}{\partial z} = \frac{h_v}{\rho_f c_{v,f} \epsilon} \left(T_b - T_f\right) + \frac{k_f}{\rho_f c_{v,f} \epsilon} \frac{\partial^2 T_f}{\partial z^2} \quad (7)$$

$$\frac{\partial T_b}{\partial t} = \frac{h_v}{\rho_b c_{v,b} (1 - \epsilon)} \left(T_f - T_b\right) \quad (8)$$

Where ρ_f is the density of the HTF, $c_{v,f}$ and $c_{v,b}$ are the volumetric specific heat of the HTF and the bed, respectively, h_v is the volumetric transmission of heat through convection, G is the mass velocity, and k_f is the thermal conductivity of the HTF.

The mathematical model, developed to simulate the behaviour of the two TES units, allows for calculation of the thermocline profile along the axial length of the tank, accounting for its variation during cyclical operation [16]. The mass flow rate of oil during both the charge and discharge phases was calculated based on the mass and energy balance equations.

2.2.5. Compressed Air Storage model

The compressed air storage (CAS) volume is calculated by solving the following system of equations:

$$\begin{cases} p_{min} V_{tot} = m_{min} R_{air} T_{st} \\ p_{max} V_{tot} = (m_{min} + \dot{m}_{air} t_{ch}) R_{air} T_{st} \end{cases} \quad (9)$$

Where p_{min} and p_{max} are the minimum and maximum air pressures, respectively, V_{tot} is the total storage volume, m_{min} is the mass of air in the cavern at minimum pressure, $\dot{m}_{air}$ is the mass flow rate of air, t_{ch} is the charge time, and T_{st} is the storage temperature inside the cavern.

https://doi.org/10.52202/069564-0187

An abandoned coal mine located in Sardinia was selected as the compressed air storage reservoir. The CAS, characterised by a depth of about 500 m and a diameter of 5 m, is assumed to be suitable for the high-pressure storage of air up to 100 bar [17]. Moreover, state-of-the-art lining of the internal volume was assumed, minimising air leakage [17]. The temperature inside the cave is set to 35 °C by the heat exchanger AC2 and was assumed to be constant during idling phases between charge and discharge phases.

In this study, a single pipe was used to transfer air from the turbomachines to the underground storage cavern and back, considering that the charging and discharge phases never occur simultaneously. The pipe is a welded steel tube, with a length of 500 m (equivalent to the distance from the surface level to the underground cavern) and an internal diameter of 0.3 m. For the sake of simplicity, the pressure losses (about 0.10-0.15 bar) were assumed to be negligible.

2.3. Power demand and production profiles

The LTA-CAES system was designed to better match the energy production of an RES power plant to the energy demand of an end-user. This section provides a comprehensive examination of the power demand profile of a small town, assumed as the end-user, and the energy generation from a wind farm and a photovoltaic plant. Subsequently, an optimisation problem is defined and solved to determine the optimal size of the LTA-CAES plant for maximum energy yield.

2.3.1. End-user electrical energy demand

The end-user in this study is assumed to be a small town with a population of about 10,000 inhabitants, for which the energy consumption data is available on a quarterly-hour base for a year. Residential, industrial, and commercial users contribute to the energy demand of the town together with the public lighting. Figure 3 displays (a) the typical load profile of the town for both a week and weekend day and (b) the overall monthly energy demand. The latter is a representative profile to be expected on a regular basis, used as reference to understand the energy consumption patterns. From Fig 3(a), it is evident that the load fluctuates rapidly throughout the day, reaching a maximum of 13.7 MW. Fig 3(b) highlights the seasonal nature of the energy demand, where energy consumption is generally higher in winter and lower in summer, except for July and August, because of the increase in energy consumption for cooling. The total annual energy demand is 64.67 GWh, with a mean monthly demand of about 5.39 GWh, as indicated by the horizontal line in Fig 3(b).

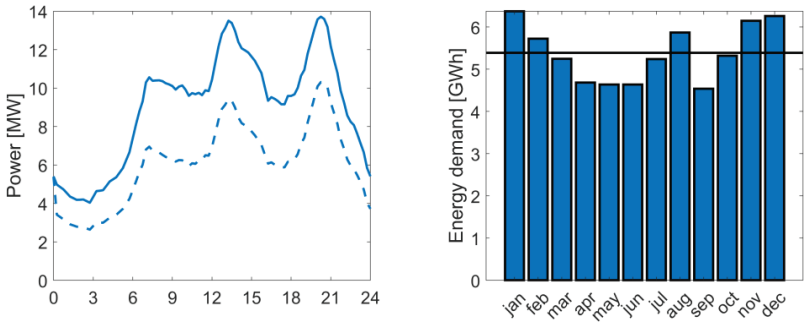

Figure. 3. (a) Load profiles for a typical week (continuous line) and weekend (dashed line) day, (b) Monthly energy demand for the entire year and average annual energy consumption.

2.3.2. Wind power production

The wind power production profile was built according to data of a real wind farm located in Sardinia. The wind farm is composed of 15 Vestas V80 wind turbines with a nominal power of 2 MW each, with a cut-in speed of 4 m/s, a cut-off speed of 25 m/s and a rated wind speed of 16 m/s. The total yearly energy production is 64.70 GWh. Figure 4 shows (a) the wind speed distribution and the wind turbine nominal power profile and (b) the overall monthly energy production of the wind farm. According to the wind speed distribution depicted in Fig 4(a), the power production of the wind turbine tends to be low throughout the year, as most of the available wind speeds fall below the turbine's cut-in speed, or at levels resulting in low energy production. Figure 4(b) shows that the monthly energy production is generally higher during winter and lower during summer, with a trend similar to that of the end-user demand displayed in Fig 3(b).

2.3.3. Photovoltaic power production

The photovoltaic power plant is based on 62,272 monocrystalline Si modules, each rated at 650 W_p, with a conversion efficiency of 20.9% [18], for a total power of 40.5 MW. The plant was modelled using the System Advisor Model (SAM) [19] software and utilising data from the NREL database [20], recorded in 2019 for a site close to Nuraxi Figus (Sardinia, Italy). Considering the various efficiency losses, the yearly energy production of a 1 MW_p plant is approximately 1.6 GWh, with a capacity factor of about 18%. Figure 5 shows (a) the typical

daily power production profile during both a summer (continuous line) and a winter day (dashed line), and (b) the monthly energy production of the PV plant. As shown in Fig 5(a), the daily power production increases in the morning, reaching a maximum around 13:00, and decreases to zero in the evening. Figure 5b shows that the energy production is greater during the summer months, revealing a seasonal nature that is inverse to that of the end-user (displayed in Fig 3(b)). For this reason, a higher surplus energy is available for the LTA-CAES system during the summer months in comparison to winter months, as discussed in the following sections.

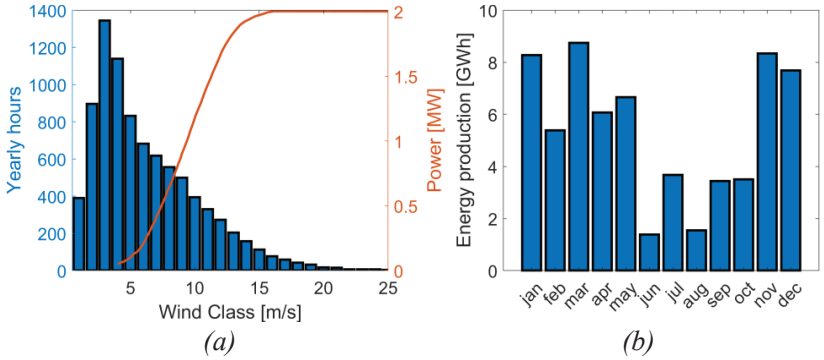

Figure. 4. (a) Wind speed distribution and wind turbine nominal power curve, (b) Monthly energy production of the wind farm.

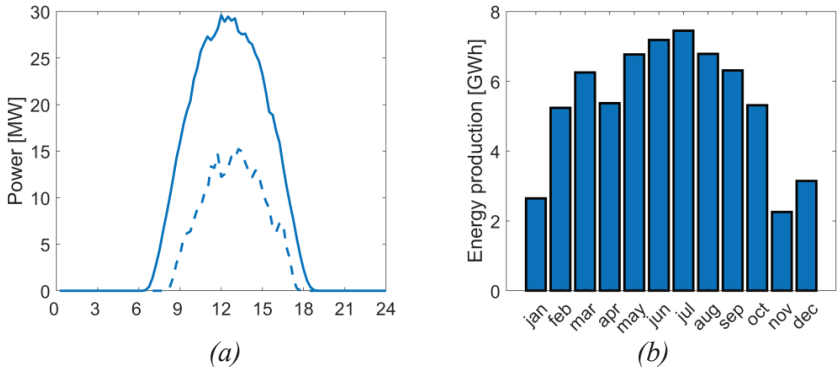

Figure. 5. (a) Power production profile of the PV plant for a typical summer (continuous line) and winter (dashed line) day; (b) Monthly energy production of the PV plant during a year.

2.4. Energy management strategy

The aim of the LTA-CAES system studied is to optimise the usage of renewable energy sources for the end-users by directly connecting the RES power plant, either photovoltaic or wind, to the end-user. Surplus RES energy is used to charge the LTA-CAES plant if the RES output exceeds the end-user's demand, and the air storage is not full. If the excess RES production cannot be stored, it is sent to the grid. On the contrary, when the RES power output is less than the end-user's demand, the LTA-CAES plant operates in discharge mode. If the total power supplied by the RES and LTA-CAES plants is still lower than the overall demand, the remaining power is sourced from the grid. Several constraints were introduced to manage the energy flows. Firstly, a limit of the maximum charge or discharge time was set to 24 hours, in order to complete a full charge or discharge of the cavern in a day or less; the charging and discharging processes have minimum power requirements to start, depending on the power required by the compressors and by the grid, respectively; buying/selling electrical energy to/from the grid during these processes was not permitted. Consequently, the charging process can only start when the available RES power is sufficient to power the compression train, and the discharging process can only start when the end-user's load demand is greater than the RES power plant production.

Due to the fluctuating nature of power production and demand profiles, the charging and discharging processes may sometimes not be completed, and they can begin or end at various cavern pressure levels. Interruptions during the charging or discharging processes also affect the thermocline profile inside the TES tank. If the charging process is terminated before full capacity, the thermocline profile stops early, causing lower air temperatures and less power output during the subsequent discharge phase. Similarly, if the discharging process cannot be completed, the thermocline profile stops early, resulting in a high level of thermal energy retained in the TES. These two phenomena occur frequently during the cyclical operation of the LTA-CAES plant and reduce the performance of the TES system and of the entire plant.

https://doi.org/10.52202/069564-0187

2.5. Optimisation

The LTA-CAES plant is designed to optimise the use of the electrical energy generated by an RES power plant by maximising the share of renewable energy consumed by the end-user. The performance and size of the plant components were evaluated based on three key design variables: the air mass flow rate of the compressor train, the charge time, and the discharge time. These design variables influence the size of the compression and expansion trains, as well as the volume of the air storage reservoir and TES units. Furthermore, these variables affect the main energy flows, including the energy used for compression, the energy produced during expansion, the energy supplied to the end-user, and the energy dispatched to the grid [21]. The optimization problem was solved with the Genetic Algorithm (GA), included in the Matlab Optimization Toolbox [22]. The three design variables were calculated to maximize the total energy sent from the LTA-CAES to the end-user, considered as the objective function. The design variables were set as integers only, and the optimization was carried out with a stopping condition of 20 generations without improvement on the best fitness function value, with default settings.

3. Results and discussion

As mentioned, this study examines the performance of an LTA-CAES plant designed to better match the energy production of an RES power plant to the energy demand of an end-user. In particular, the LTA-CAES design variables have been evaluated for an RES power plant based either on a PV power plant or a wind farm. The results are presented in Table 2.

Table 2. Optimal design parameters for the analysed LTA-CAES plants.

	PV	Wind
Mass flow rate (kg/s)	24	16
Charge time (h)	10	24
Discharge time (h)	24	24

The results of the optimisation process are used to determine the size of the LTA-CAES plant. The size of the plant can be characterised by the input and output power of the plant, the volume of the TES units, and the length of the cavern (considering a diameter of 5 m). Table 3 shows the size of the main components of the plant. For the system coupled with the wind farm, the entire energy storage system (TES and cavern) is characterised by a larger volume, thus storing more energy. For the system coupled with the PV plant, the optimisation process results in a higher input power and lower output power compared to the system coupled with the wind farm. In the case of the PV, the surplus power is high, and the power demand is low, resulting in a high input power and low output power for the LTA-CAES plant.

Table 3. Main parameters for the LTA-CAES combined with a PV or wind power plant.

	Input power [MW]	Output power [MW]	TES1 volume [m^3]	TES2 volume [m^3]	Cavern length [m]
PV	14.9	4.2	1005	1683	1655
Wind	9.9	6.7	1683	2613	2647

The energy balances of the system were solved with a time step of 15 minutes for one year, considering the power output of the two RES plants and the power demand of the end-user. The performance of the compression and expansion trains of the LTA-CAES plant, throughout the full charge and discharge phases, is illustrated in Fig 6, where the reference power, denoted as P_{ref}, represents the nominal power of the turbomachine. This plot shows the generalised power (the ratio between the actual power and the reference power) as a function of the charge level of the storage volume. During the charge and discharge phases, variations in pressure within the cavern and temperature within the TES systems cause variations of the compression and expansion power. It can be observed that the power variation is limited: the compressors power curve shows a steady increase of about 8.4% throughout the charge phase, while the turbine power production remains mostly constant, decreasing only by 2.9% at the end of the discharge phase. The compressor profile increase is mainly due to the increase in the HPC compression power, as shown in Fig 6(a). The compression ratio increases from 1.31 to 1.87 during the charge phase, leading to a subsequent increase in the required compression power. The power curve shows a steady increase due to the relatively small variation in efficiency, ranging between 69% and 80%. Furthermore, most of the compression energy (88%) is required by the LPC, MPC1, and MPC2 that operate at design conditions, while the HPC is responsible for the remaining share of the total compression work. The power output of the turbines, shown in Fig 6(b), remains constant until it starts to drop towards the end of the discharge phase. This power reduction is caused by the temperature reduction at the outlet of the TES units. As the HPT and MPT operate at design condition, their polytropic efficiency remains constant. Similarly, the efficiency of the LPT is mostly constant since the variation in power of the turbines is low.

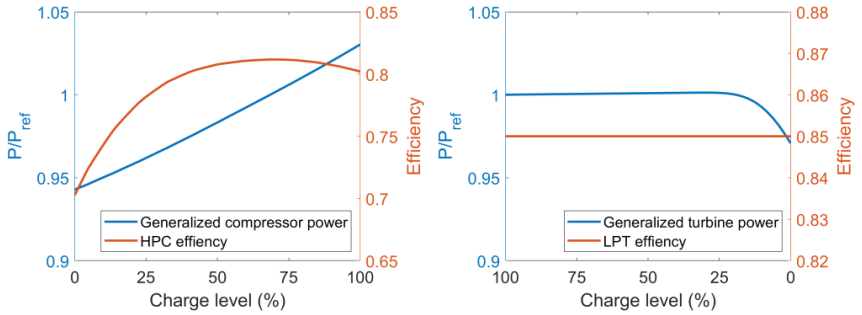

Figure. 6. (a) Generalised total compressor power and HPC efficiency during the charge phase and (b) Generalised total power production of the turbine train and LPT efficiency.

Figure 7 shows the key temperature profiles throughout a complete discharge phase and its evolution over fifty charge and discharge cycles. The temperature profile at the turbine inlet is shown in Fig 7(a) for the LPT, in Fig 7(b) for the MPT, and in Fig 7(c) for the HPT. The reduction in temperature towards the end of the discharge phase is responsible for the power reduction depicted in Fig 6(b). During the discharge phase of the first cycle, a substantial temperature decrease is observed. However, the minimum temperature gradually increases with each cycle, ultimately reaching a saturation state after about 50 cycles. Figures 7(b) and 7(c) additionally show the temperature difference between the inlet and the outlet (coincident with the turbine inlet) of the heat exchangers. By comparing the maximum temperature in Fig 7(a) with those of Fig 7(b) and 7(c), it is evident that the direct TES (TES1) results in improved energy utilisation. This is due to the fact that the indirect heat transfer section involves two temperature drops: one for the heat exchangers of the charge section (IC1 and IC2) and one for the heat exchangers of the discharge section (HX1 and HX2).

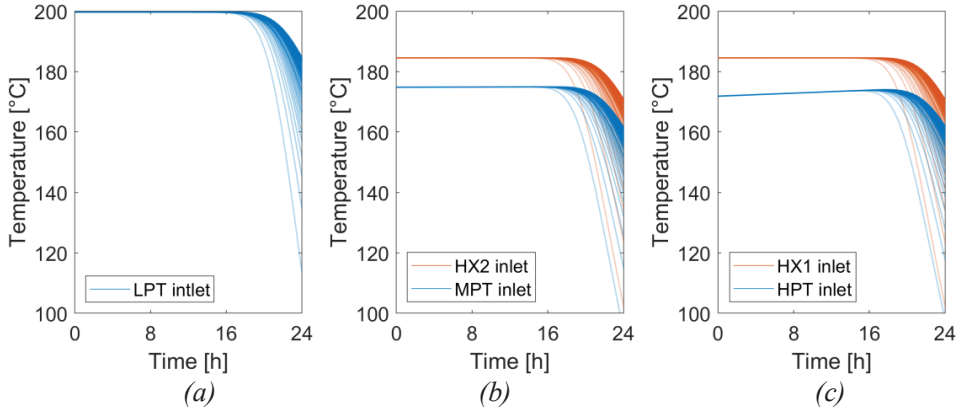

Figure. 7. Temperature profile during the discharge phase and its evolution over fifty full charge and discharge cycles at (a) the LPT inlet, (b) the MPT inlet (blue) and HX2 inlet (red), and (c) the HPT inlet (blue) and HX1 inlet (red).

Figure 8 represents the power production profile of the PV plant, the power demand profile of the end-user, and the input and output power profiles of the LTA-CAES plant, for both a typical high irradiance day (Fig 8(a)) and a low irradiance day (Fig 8(b)). During the daytime, when the PV power production (in blue) exceeds the demand (in orange) and is sufficient to drive the compressors, the excess energy is stored by the LTA-CAES (in yellow) for later use during the night (in purple), when the PV plant is not generating power. On a high irradiance day (typically during summer), the LTA-CAES plant can store enough energy during the day to meet the entire end-user demand during the night. In contrast, during a low irradiance day (typically during winter), the plant cannot fully satisfy the end-user demand.

Figure 9 displays the power production profile of the wind power plant, the power demand profile of the end-user, and the input and output power profiles of the LTA-CAES plant, for both a high wind speed day (Fig 9(a)) and low wind speed day (Fig 9(b)). Unlike the PV plant, the power production profile of the wind farm is highly variable, resulting in a less predictable behaviour of the LTA-CAES system. During a windy day (Fig 9(a)), the power generated by the wind power plant is sufficient to meet the end-user demand and fully charge the LTA-CAES system, which stores the excess energy for later use since the energy produced by the RES power plant is enough to cover the energy demand of the end-user. In contrast, during a low wind speed day (Fig 9(b)), the power production is lower, making it difficult for the LTA-CAES system to satisfy the end-user demand. The energy stored inside the CAES is enough to cover only a part of the demand of the end-user (in

https://doi.org/10.52202/069564-0187

purple). Unlike in the case of the PV plant, when the LTA-CAES is coupled with the wind power plant, the charge and discharge phase are not dependent on the time of day, since the wind power plant can generate energy throughout the day and night.

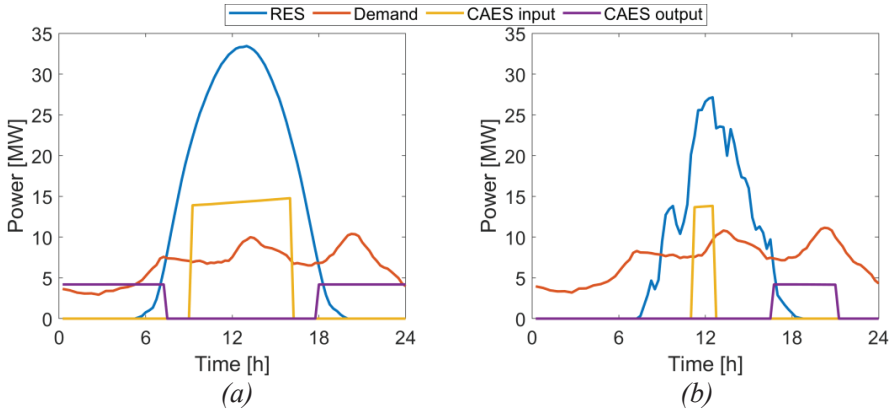

Figure. 8. Main power flows of the LTA-CAES plant for a high irradiance day (a) and a low irradiance day (b), when combined with a PV power plant.

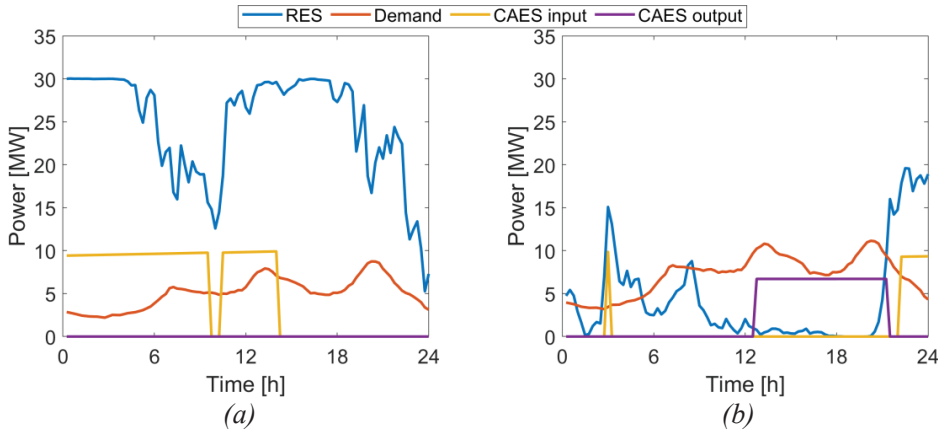

Figure. 9. Main power flows of the LTA-CAES plant for a high wind speed day (a) and a low wind speed day (b), when combined with a wind power plant.

Based on the power production and demand profiles, the mathematical simulation of the system allows evaluation of the operation of the LTA-CAES plant throughout the year. Figure 10, where the level of charge in the cavern is shown for the entire year, illustrates that the charging and discharging processes are frequently interrupted and rely heavily on power availability and demand throughout the day. As demonstrated in Fig 10(a), during the summer, the PV plant generates more energy than the end-user requires, resulting in surplus power that allows the LTA-CAES plant to charge more frequently. Conversely, during the winter, the PV plant's energy production is insufficient, and the LTA-CAES plant must compensate for the deficit. The trend is almost reversed for the wind plant in Fig 10(b), where production is greater during the winter.

Figure 11 shows the yearly energy balance of the system, where the yearly energy demand of the users amounts to 64.6 GWh. When coupled with the PV plant, the LTA-CAES system can supply a total of 39.2 GWh to the end-users (60.7% of the yearly energy demand). In particular, 41.8% of the total energy demand is directly provided by the PV plant and 18.9% by the LTA-CAES system, while the remaining 39.3% is covered by the grid. When coupled with the wind farm, the LTA-CAES is capable of supplying a total of 36.7 GWh of energy to the end-user (56.5% of the yearly energy demand). In this case, 48.0% of the energy demand is provided by the wind farm and the 8.4% by the LTA-CAES system, while the remaining 43.6% by the grid. The total energy produced by the LTA-CAES is 13.5 GWh and 8.0 GWh when coupled with the PV and the wind farm, respectively. The share of energy produced by the LTA-CAES and sent directly to the users is 90.6% and 68.2% for the plant coupled with the PV and the wind farm respectively, while the remaining produced energy is sent to the grid. The amount of energy produced and sent directly to the grid is higher for the system coupled with the wind farm, because the output power of the system is higher than the end-user power demand. The round-trip efficiency is about 67% for both plants. For the LTA-CAES coupled with the PV, the total charge time is equal to 1,388 h/year and the total discharge time is 3,328 h/year. For the LTA-CAES

coupled with the wind farm, the total charge and discharge time is 1,235 h/year. The total energy production of the LTA-CAES system coupled with the PV plant exceeds that of the system coupled with the wind farm by 8%. Hence, coupling the LTA-CAES system with the PV plant appears to be the optimal choice in terms of energy efficiency. Furthermore, the system coupled with the PV plant has a higher share of energy produced by the LTA-CAES and sent directly to the end-users compared to the system coupled with the wind farm. This suggests that the former configuration enables a greater degree of energy self-sufficiency for the end-user.

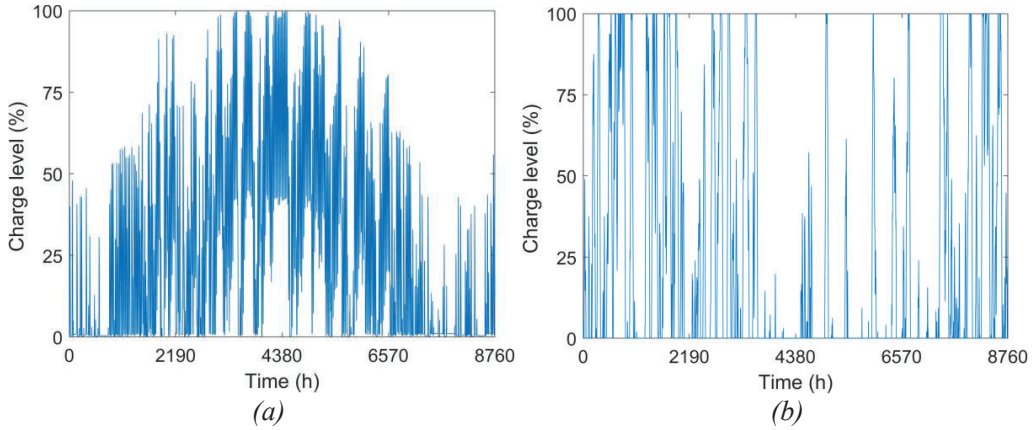

Figure. 10. Yearly charge level of the cave coupling the CAES system with a) PV or b) wind farm.

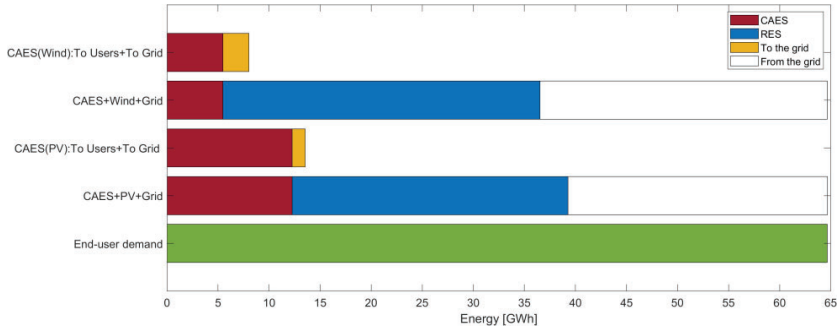

Figure. 11. Energy production from the LTA-CAES plant, coupled with a wind or a PV power plant, compared to the total annual energy demand of the end-user.

4. Conclusions

This paper proposed an LTA-CAES configuration for efficient utilisation of the electrical energy between an RES power plant and a small town in Sardinia. The plant configuration utilised readily available components in order to minimise costs and ensure efficient operation of the turbomachines during both charging and discharge phases. This was achieved by fixing the mass flow rate of air, allowing most of the compressors and turbines to operate at constant speed and at design conditions. The plant features two TES units to store the thermal energy while maintaining a low operative pressure inside the tanks. A dedicated circuit for the heat transfer oil is utilised in combination with heat exchangers to guarantee optimal working conditions for the turbomachines. To account for pressure and temperature variations during discharging, a throttling valve is located at the inlet side of each turbine. Mathematical models were developed to correctly size the plant and to simulate its operation under different conditions, accounting for off-design performance of the various components, i.e., the turbomachines, the TES units, and the heat exchangers.

Simulation results demonstrated the effectiveness of the proposed integrated LTA-CAES plant in managing energy production and consumption over the course of a year, when coupled with wind or photovoltaic power plants. With a wind power plant, a larger share of energy can be directly supplied to the end-user compared to the PV power plant. However, the LTA-CAES system coupled with the PV plant yields a higher total energy production. In fact, the results show that the LTA-CAES system increases the share of renewable energy supplied to the end-user from 41.8% to 60.7% when coupled with the PV plant, and from 48.0% to 56.5% when coupled with the wind farm.

Overall, the system was shown to be a viable low-emission energy management solution for a small community of about 10,000 people on the island of Sardinia. To increase the performance of the system, an integration of

https://doi.org/10.52202/069564-0187

the PV and wind power plants will help to determine the optimal RES plant configuration to be coupled with an LTA-CAES plant. Moreover, the development of a techno-economic analysis of the components of the plant will allow determination of the overall cost of the system.

Acknowledgements

This research was carried out as part of a project entitled “Advanced Energy Storage Systems for Sustainable Communities”, funded by the University of Cagliari with financial support from Fondazione di Sardegna, Year 2019 (CUP F72F20000340007).

Nomenclature

A heat exchangers area, m^2
c specific heat capacity, J/(kgK)
G mass velocity, kg/(m^{2}s)
h volumetric heat transfer coefficient, W/(m^{3}K)
k thermal conductivity, W/(mK)
m mass, kg
$\dot{m}$ mass flow rate, kg/s
n rotational speed, rpm
p pressure, bar
$\dot{Q}$ exchanged thermal power, W
R gas coefficient, J/(kg K)
t time, s
T temperature, K
U heat transfer coefficient, W/(m^3 K)
V storage volume, m^3
z axial position, m

Greek symbols

β pressure ratio
γ specific heat capacity ratio
ϵ bed void fraction
η polytropic efficiency
ρ density, kg/m^3

Subscripts and superscripts

b bed
c compressor
ch charge phase
dis discharge phase
f fluid
in inlet
max maximum
min minimum
ML medium logarithmic
out outlet
p pressure
ref reference
rid reduced
t turbine
v volume

References

[1] Ould Amrouche S, Rekioua D, Rekioua T, Bacha S. Overview of energy storage in renewable energy systems. Int J Hydrog Energy. 2016 Dec;41(45):20914–27.

[2] Kousksou T, Bruel P, Jamil A, El Rhafiki T, Zeraouli Y. Energy storage: Applications and challenges. Solar Energy Materials and Solar Cells. 2014 Jan;120:59–80.

[3] Budt M, Wolf D, Span R, Yan J. A review on compressed air energy storage: Basic principles, past milestones and recent developments. Appl Energy. 2016 May;170:250–68.

[4] Wolf D, Budt M. LTA-CAES – A low-temperature approach to Adiabatic Compressed Air Energy Storage. Appl Energy. 2014 Jul;125:158–64.

[5] Grazzini G, Milazzo A. Thermodynamic analysis of CAES/TES systems for renewable energy plants. Renew Energy. 2008 Sep;33(9):1998–2006.

[6] Hartmann N, Vöhringer O, Kruck C, Eltrop L. Simulation and analysis of different adiabatic Compressed Air Energy Storage plant configurations. Appl Energy. 2012 May;93:541–8.

[7] Wang S, Zhang X, Yang L, Zhou Y, Wang J. Experimental study of compressed air energy storage system with thermal energy storage. Energy. 2016 May;103:182–91.

[8] Zhang Y, Xu Y, Zhou X, Guo H, Zhang X, Chen H. Compressed air energy storage system with variable configuration for accommodating large-amplitude wind power fluctuation. Appl Energy. 2019 Apr;239:957–68.

[9] Arabkoohsar A, Rahrabi HR, Alsagri AS, Alrobaian AA. Impact of Off-design operation on the effectiveness of a low-temperature compressed air energy storage system. Energy. 2020 Apr 15;197.

[10] Tola V, Marcello FC, Cocco D, Cau G. Performance Assessment of Low-Temperature A-CAES (Adiabatic Compressed Air Energy Storage) Plants. Journal of Thermal Science. 2022 Sep 20;31(5):1279–92.

[11] Casey M, Robinson C. A Method to Estimate the Performance Map of a Centrifugal Compressor Stage. J Turbomach. 2012 Nov 8;135(2).

[12] Balje´ OE. A Study on Design Criteria and Matching of Turbomachines: Part A—Similarity Relations and Design Criteria of Turbines. Journal of Engineering for Power. 1962 Jan 1;84(1):83–102.

[13] Therminol-66 - Available online:<https://www.therminol.com/product/71093438> [accessed 14.3.2023].

[14] R. K. Sinnott. Chemical Engineering Design. Vol. 6. Pergamon Press; 1996.

[15] Cascetta M, Serra F, Cau G, Puddu P. Comparison between experimental and numerical results of a packed-bed thermal energy storage system in continuous operation. In: Energy Procedia. Elsevier Ltd; 2018. p. 234–41.

[16] Cascetta M, Cau G, Puddu P, Serra F. Numerical investigation of a packed bed thermal energy storage system with different heat transfer fluids. In: Energy Procedia. Elsevier Ltd; 2014. p. 598–607.

[17] Okuno T, Wakabayashi N, Niimi K, Kurihara Y, Iwano M. Advanced natural gas storage system and verification tests of lined rock cavern-ANGAS project in Japan. International Journal of the JCRM. 2009;5(2):95–102.

[18] Vertex DE21 - Available online:<https://www.trinasolar.com/it/product/VERTEX-DE21> [accessed 15.3.2023].

[19] System Advisor Model Version 2022.11.21 (SAM 2022.11.21). National Renewable Energy Laboratory. Golden, CO.

[20] NSRB. National Solar Radiation Database. – Available at:<https://nsrdb.nrel.gov/data-viewer> [accessed 15.3.2023].

[21] Cocco D, Licheri F, Micheletto D, Tola V. ACAES systems to enhance the self-consumption rate of renewable electricity in sustainable energy communities. J Phys Conf Ser. 2022 Dec 1;2385(1):012025.

[22] Optimization Toolbox version: 9.4 (R2022b), Natick, Massachusetts: The MathWorks Inc.; 2022.

 https://doi.org/10.52202/069564-0187